Phase retrieval for a complex-valued object by using a low-resolution image

J. R. Fienup and A. M. Kowalczyk

Optical Science Laboratory, Advanced Concepts Division, Environmental Research Institute of Michigan, P.O. Box 8618, Ann Arbor, Michigan 48107

Received July 28, 1989; accepted November 9, 1989

It is difficult to reconstruct an image of a complex-valued object from the modulus of its Fourier transform (i.e., retrieve the Fourier phase) except in some special cases. By using additionally a low-resolution intensity image from a telescope with a small aperture, a fine-resolution image of a general object can be reconstructed in a two-step approach. First the Fourier phase over the small aperture is retrieved, using the Gerchberg–Saxton algorithm. Then that phase is used, in conjunction with the Fourier modulus data over a large aperture together with a support constraint on the object, to reconstruct a fine-resolution image (retrieve the phase over the large aperture) by the iterative Fourier-transform algorithm. The second step requires a modified algorithm that employs an expanding weighting function on the Fourier modulus.

1. INTRODUCTION

Phase retrieval from a single intensity distribution for the case of complex-valued objects arises in a number of applications such as holography, wave-front sensing, and imaging with coherent illumination. If the support of the object (the set of points over which it is nonzero) is well known or of a favorable type, then it is often possible to reconstruct an image of the object from the modulus of its Fourier transform (the square root of the Fourier intensity) by using the iterative Fourier-transform algorithm.[1] Favorable support constraints include polygons with no parallel sides (particularly triangles), which must be known *a priori*,[1,2] and supports with separated parts, which need not be known *a priori*.[1,3] If, on the other hand, the object has a polygonal support that is not known well *a priori*, or if the object has tapered edges (i.e., it goes to zero smoothly, rather than abruptly, at its edges), then both the ability to converge to a solution and the quality of the reconstructed image deteriorate.[1,4–6] This situation contrasts sharply with the case of real, nonnegative objects, for which phase retrieval is much easier.[7–9] Image reconstruction is also possible if the complex-valued object has a strong glint or glints (for example, a single glint well separated from the object gives rise to a hologram that can be reconstructed easily[10]).

In this paper we show that even the difficult types of complex-valued objects can be reconstructed if one has a low-resolution intensity image of the object, taken through a telescope having a small aperture contiguous with the Fourier intensity measurements, to supplement the Fourier intensity data. In Section 2 an example is given of an optical system that would produce the desired measurements. Section 3 describes the data-processing steps required to reconstruct a fine-resolution image. A two-step method is used, employing an accelerated version of the Gerchberg–Saxton algorithm[11–15] in the first step and a modified version of the iterative Fourier-transform algorithm[1,7–9,13–15] in a second step. This new modification, the expanding weighted modulus algorithm, was necessary to produce convergence with a reasonable number of iterations. In Section 4 an example of reconstructing an image by using this approach is given, and Section 5 contains our conclusions.

2. OPTICAL SENSOR CONFIGURATION

Suppose that the object being imaged is illuminated by a coherent laser and is far away so that the relationship between the optical field at the object, $f(x)$, and that in the aperture plane of the optical receiver, $F(u)$, is approximately a Fourier transform.[16] Here u and x are both two-dimensional coordinates: u in the aperture plane and x in the object or image plane. (If the relationship is a Fresnel transform, then the method described here will work with minor modifications.[17]) Figure 1 depicts an example of an optical receiver that gathers the types of data needed for the reconstruction described here. An array of light-bucket detectors (shown with field lenses in front of them) samples the intensity of the optical field in the aperture plane. For the intensity of the speckle pattern in the aperture plane to be sampled adequately, there must be at least two detectors per speckle width in each dimension (as determined by the wavelength of the laser, the distance to the object, and the object diameter). Since only the intensity is detected, these measurements are independent of any phase errors that may be present owing to atmospheric turbulence in front of the aperture (assuming that atmospheric scintillation is negligible) or owing to misalignment of the detector array. In addition, embedded in the array (or contiguous with the array on the edge of the array) is a small-aperture diffraction-limited telescope. If it is located on Earth, the small-aperture telescope could be diffraction limited by virtue of having an adaptive-optics system that compensates for atmospheric turbulence in real time. Such an adaptive-optics system may not be practical for a telescope with an aperture the size of the entire large aperture. If it is in space, then adaptive optics would not be needed for the small telescope. A beam splitter in the small telescope allows for the detection of intensity simultaneously in two planes: the usual

0740-3232/90/030450-09$02.00

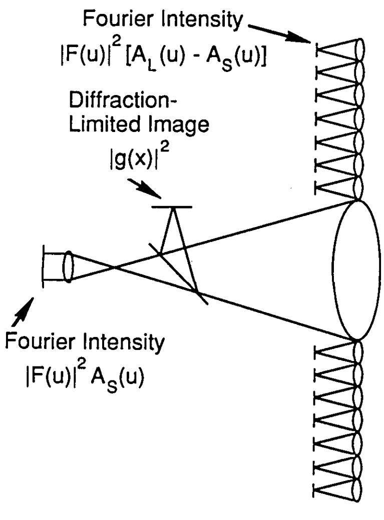

Fig. 1. Optical sensor configuration. Data collected for a coherently illuminated object (not shown, located far to the right) include aperture-plane (Fourier) intensity and a low-resolution diffraction-limited intensity image from a small-aperture telescope.

focal plane, where there exists a diffraction-limited image of the object, and a demagnified image of the aperture plane. The diffraction-limited image of the object has low resolution since it comes from a small aperture. It is assumed that the intensity measurements are made over a short enough time that the object and the receiver are essentially fixed in space relative to each other.

In summary, the optical receiver makes the following intensity measurements: Letting A_L (a binary function) denote the entire large aperture (including the small aperture) and A_s denote the small aperture, we have $|F(u)|^2[A_L(u) - A_s(u)]$ from the light-bucket detectors, $|F(u)|^2A_s(u)$ from the reimaged aperture of the small telescope, and $|g(x)|^2$, the intensity of the low-resolution image, where $g(x) = a_s(x) * f(x)$, $a_s(x)$ is the Fourier transform of $A_s(u)$, and $*$ denotes convolution.

3. DATA-PROCESSING STEPS

Figure 2 is a block diagram depicting how these three intensity measurements (or their square roots, the moduli or magnitudes) are used to retrieve the phase over the large aperture and recontruct a fine-resolution image. A support constraint for the object is computed (in either of two ways), and the phase over the small aperture is retrieved. Then the fine-resolution image is reconstructed by using all the available information. In what follows, each of these steps is described in some detail.

A. Support Estimation

Assuming that the object, which is flood illuminated by a laser, is on a dark background, a support constraint for the object can be obtained in one of two ways: from the low-resolution image or by using a triple intersection of the autocorrelation support.[3,18]

An estimate of the support of the object can be obtained from the low-resolution image, $|g(x)|^2$, by thresholding it at an appropriate level [i.e., the support function is set equal to unity where $|g(x)|^2$ exceeds the threshold and to zero elsewhere]. If the threshold level is set too high, then the support of the object is underestimated. If the threshold level is set too low, then the support is overestimated because of noise and sidelobes owing to diffraction. The sidelobes can be minimized by placing an apodization (weighting) across the small aperture but at the expense of optical efficiency and resolution of the low-resolution image.

The method that we find useful for selecting the threshold level is as follows. Several candidate thresholded low-resolution images are computed by using different threshold values. When the threshold value is too high, small changes in the threshold value tend to cause small changes in the area of the thresholded image. When the threshold falls below the value needed to pick up the noise and/or sidelobes, then the area of the thresholded image grows rapidly, spreading over the entire image space, and the thresholded image breaks up rapidly. This is illustrated by the example shown in Fig. 3 for the case of a telescope with a small circular aperture (a diameter-16 circle embedded in a 128 × 128 array). Thus a good choice of threshold value is one just larger than the values for which the area of the thresholded image grows rapidly. Figure 4 shows the corresponding results for the case of a weighting function across the small aperture. The weighting function was chosen to be the autocorrelation of a circle of half the diameter of the small aperture; that is, the weighting function falls to zero at the edges of the small aperture. With the aperture weighting included, the diffraction sidelobes are greatly reduced, and the area of the thresholded image is much less sensitive to changes in the threshold value, making the aperture weighting worthwhile despite the loss of resolution that it causes.

For the case of diffusely scattering objects, the Fourier intensity is a speckle pattern, and the image (the low-resolution image as well as the fine-resolution image) is speckled,[19] as can be seen from Figs. 3 and 4. Nulls in the thresholded image due to speckle nulls in $|g(x, y)|^2$ can be eliminated by convolving the thresholded image with a small circle and then rethresholding, as illustrated in Fig. 5. The estimate of

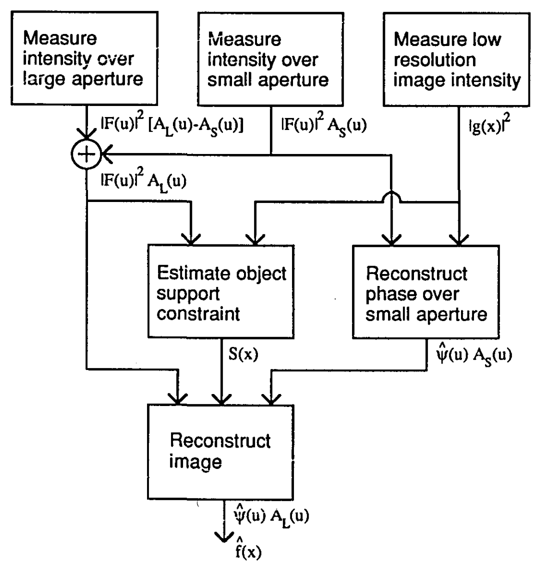

Fig. 2. Data-processing steps to reconstruct a fine-resolution image (retrieve the phase in the aperture plane) from the intensity measurements.

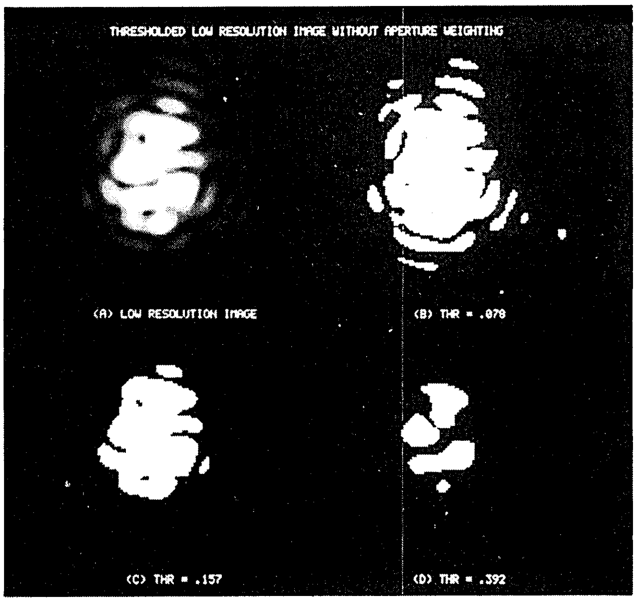

Fig. 3. Thresholding the low-resolution intensity image to estimate a support constraint, with no weighting on the small aperture. (A) Diffraction-limited low-resolution image modulus (overexposed in order to show the sidelobes that extend beyond the support of the object); (B)–(D) thresholded images, with threshold values equal to (B) 0.078, (C) 0.157, and (D) 0.392 of the maximum value of the image.

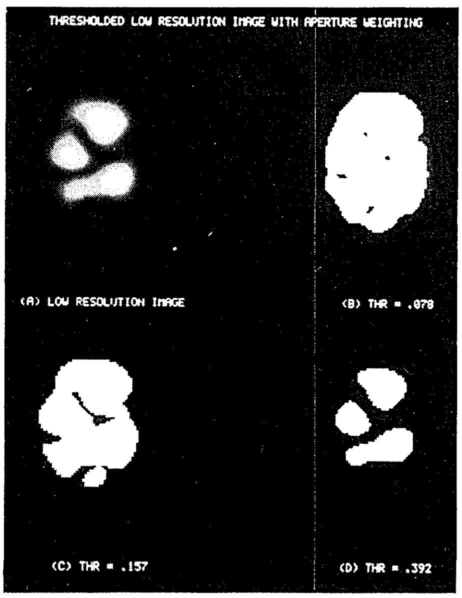

Fig. 4. Thresholding the low-resolution intensity image to estimate a support constraint, with a weighting on the small aperture. (A) Diffraction-limited low-resolution image (not overexposed); (B)–(D) thresholded images, with threshold values equal to (B) 0.078, (C) 0.157, and (D) 0.392 of the maximum value of the image.

the support of the object, shown in Fig. 5(C), is used as a support constraint in the final step of fine-resolution image reconstruction by the iterative Fourier-transform algorithm. Since this support constraint is only approximate and may be too small, it is often useful to enlarge the support constraint to ensure that the object fits within it. We typically enlarge the support constraint by adding pixels to the edges of the initial support constraint, as shown by the example in Fig. 5(D).

A second method of generating a support constraint, which uses the Fourier intensity over the entire aperture, is the method of triple intersection of the autocorrelation support.[3] First the Fourier intensities over the small aperture and from the light-bucket detectors are combined to arrive at the intensity over the entire aperture. This intensity is inverse Fourier transformed to obtain a fine-resolution (complex-valued) autocorrelation of the object. The magnitude of the autocorrelation function is thresholded, and the nulls due to speckles are eliminated in a way similar to that shown in Fig. 5. Noise and sidelobes outside the true autocorrelation support are eliminated to the extent possible by a similar method operating on the complement of the support. The result is an estimate of the support of the autocorrelation. Then three appropriate translates of the autocorrelation support are made to intersect to arrive at an upper bound on the support of the object.[3] In this case the support constraint is not an estimate of the support of the object but is an upper bound that contains all possible object supports consistent with the support of the autocorrelation.

The support constraint computed from the autocorrelation function is from finer-resolution data and therefore may be more accurate, but it may also be too large since reconstruction of the support of an object from the support of its autocorrelation function is ambiguous for wide classes of objects.[3,20] The thresholded low-resolution image avoids these ambiguity problems but, being of lower resolution, may not be so accurate. Further study is required to determine which of the two methods is better and to devise a way to combine the best features of each into a composite support estimate.

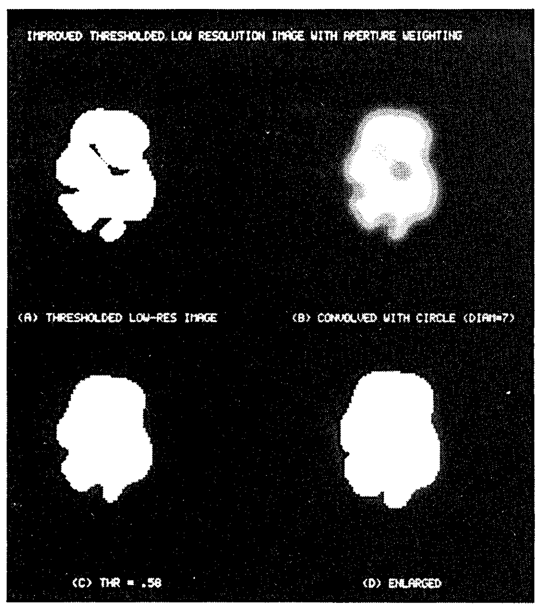

Fig. 5. Removal of nulls due to speckles in the image. (A) Thresholded image from Fig. 4(C), (B) convolution of (A) with a circle of diameter 7 pixels (about half the diameter of a speckle), (C) thresholding of (B) at 0.58 of its peak, (D) enlarged version of (C) that may be used to ensure that the object fits within it.

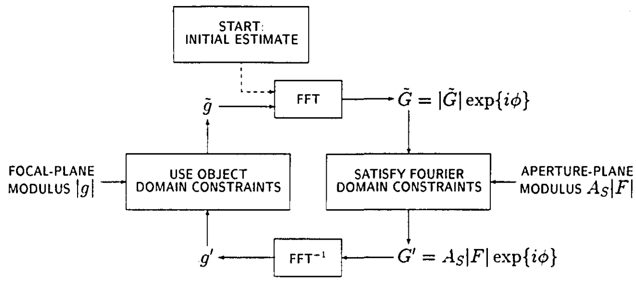

Fig. 6. Block diagram of the Gerchberg–Saxton algorithms. The object-domain constraint is the square root of the measured intensity of the low-resolution image, and the Fourier constraint is the square root of the measured intensity over the small aperture. FFT denotes fast Fourier transform.

B. Small-Aperture Phase Retrieval Using The Gerchberg–Saxton Algorithm

The phase, $\psi(u)$, of the optical field, $F(u)A_s(u)$, in the plane of the small aperture is determined from the intensities in the focal plane and the image of the aperture plane by using a variation of the Gerchberg–Saxton algorithm that is accelerated. Figure 6 is a block diagram for the Gerchberg–Saxton algorithms. Here we refer to the original Gerchberg–Saxton algorithm[11,12] as GS and the accelerated versions as GS1 and GS2,[13–15] the latter having the image-domain operation[14] [combining Eqs. (9) and (10) of Ref. 14]

$$\tilde{g}_{k+1}(x) = g_k' + \beta\left[2|g(x)|\frac{g_k'(x)}{|g_k'(x)|} - g_k'(x) - |g(x)|\frac{\tilde{g}_k(x)}{|\tilde{g}_k(x)|}\right], \tag{1}$$

where β is a constant, $|g(x)|$ is the modulus of the low-resolution image, $\tilde{g}_k(x)$ is the input image to the kth iteration, and $g_k'(x)$ is the output image from the kth iteration. The rates of convergence for these three algorithms were compared, and β was optimized. The differences in the convergence rates are affected not only by the choice of β but also by the choice of the random phase used as the initial estimate. It was found that GS2 generally converges much faster than GS1, which in turn converges significantly faster than GS. A better method than using any single algorithm is to combine GS2 and GS: perform several iterations with GS2, which initially converges quickly, then finish with several iterations of GS, which is more stable and converges to a smaller error. For these algorithms the object-domain error metric (ODEM), a normalized root-mean-squared (rms) error, is given by

$$\mathrm{ODEM}^2 = \frac{\sum_x [|g_k'(x)| - |g(x)|]^2}{\sum_x |g(x)|^2}, \tag{2}$$

which is a measure of how closely the output image modulus agrees with the modulus of the measured low-resolution image and is the criterion by which we judge whether the algorithm has converged. (A similar error metric in the Fourier domain can also be used.) Note that in order for Eq. (2) to be meaningful it is necessary to normalize $|g(x, y)|$ so that it has the same energy (sum of squares) as the Fourier modulus data. The quality measure that we use to evaluate the reconstruction results is the absolute error (ABSERR) of the complex-valued reconstructed image, also a normalized rms error, which is given by

$$\mathrm{ABSERR}^2 = \frac{\sum_x |\alpha g'(x - x_0) - g(x)|^2}{\sum_x |g(x)|^2}, \tag{3}$$

where α is the complex factor and x_0 is the shift that minimizes the ABSERR. It can be shown that x_0 is given by the location of the maximum magnitude of $r_{g'g}(x)$, the cross correlation of g' with g; and $\alpha = r_{g'g}(x_0)/\sum|g'(x)|^2$. This ABSERR can be computed only in digital simulation experiments for which the true image is known. Although it measures the error in the complex numbers, which includes both magnitude and phase errors, the ABSERR correlates well with the standard deviation, σ_ϕ, of the error of the phase retrieved over the small aperture. As is shown in Appendix A, the expected relationship, if errors in the modulus are ignored, is

$$\mathrm{ABSERR}^2 \simeq 1 - \exp(-{\sigma_\phi}^2). \tag{4}$$

Figure 7 shows examples of algorithm convergence. Twenty iterations of either GS2 or GS were followed by twenty iterations of GS. The optimum value of β was found to be approximately 1.5 to 2. The algorithm is not highly sensitive to small changes in the value of β. Retrieval of the phase over the small aperture was found to be relatively fast (only ~30 iterations are required).

To test the sensitivity of the combined algorithm to noise, low light levels (quantum-limited measurements) were simulated by subjecting the intensity measurements in both planes to a Poisson noise process. We chose to simulate the same number of photons in each of the two planes. After the

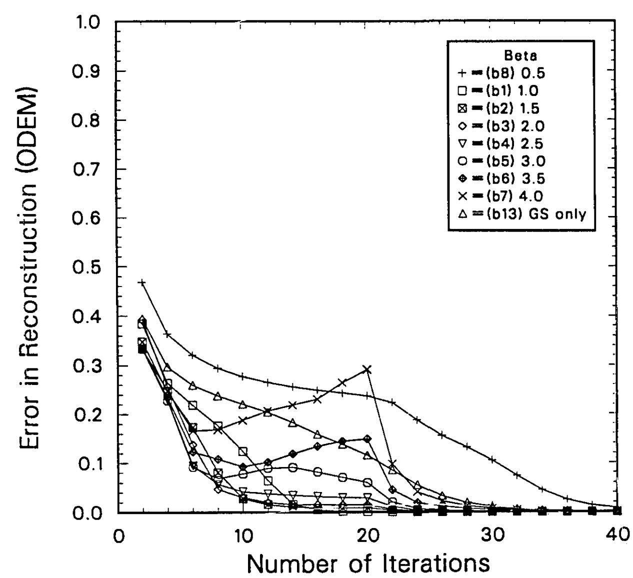

Fig. 7. Convergence of the Gerchberg–Saxton (GS) and accelerated Gerchberg–Saxton (GS2) algorithms. Twenty iterations of either GS2 or GS were followed by twenty iterations of GS. GS2 with feedback parameter $\beta = 1.5$ to $\beta = 2$ converged fastest.

intensity data were scaled to have a given expected total number of detected photons, each pixel was replaced with a sample drawn from a Poisson distribution with mean and variance equal to the pixel value.

For these experiments the object is approximately of size 40×60 pixels embedded in a 128×128 array. Therefore the intensity of the Fourier transform of the object (computed using a fast Fourier transform) is a speckle pattern with approximately 3×2 samples per speckle. The Fourier data were set to zero outside a circle of diameter 16 pixels to simulate the effect of the small aperture (without weighting). Therefore there should be $\pi 8^2/6 \simeq 33$ speckles in the small aperture.

Figure 8 shows the ABSERR, the quality of the output image, as a function of iteration number for a variety of noise levels. Figure 9 shows the ABSERR for the reconstructed image as a function of the total number of detected photons. Good results are obtained for 10^4 or more photons, corresponding to $10^4/33 \simeq 300$ photons per speckle. From these results we see that the Gerchberg–Saxton algorithms converge rapidly and are reasonably robust in the presence of noise.

Since the image domain was highly oversampled, we also performed a simple noise filtering before reconstructing with the GS algorithm. The noisy image intensity was Fourier transformed, the Fourier transform was set to zero outside a circle of diameter 32 pixels (since the ideal complex-valued image has a Fourier transform that is zero outside a circle of diameter 16 pixels), and the result was inverse Fourier transformed to yield a smoothed image with reduced noise. Before the square root was taken to compute the image modulus, small negative numbers introduced by the filtering process were set to zero. As expected, we found that the ODEM was lower for the reconstructions with noise filtering than without it. However, the ABSERR, which is ultimately of greater importance, was slightly better without filtering; consequently it is better not to filter the image in this instance. This subject of filtering requires further analysis.

C. Fine-Resolution Image Reconstruction

With all the data in hand—including the Fourier intensity over the entire aperture, the phase over the small aperture, and the support constraint—we perform image reconstruction by using the iterative Fourier-transform algorithm, which seeks a solution consistent with all the data and constraints.[1,7–9,13–15] A block diagram of the algorithm, which is a generalization of the Gerchberg–Saxton algorithm, is shown in Fig. 10.

When using any phase information in the Fourier domain, one must choose the position of the support constraint in the image domain to be consistent with the given Fourier phase. (For more conventional phase retrieval with no *a priori* phase information, the position does not matter.) One way to ensure correct positioning is to cross correlate the support constraint with the low-resolution image and use the location of the peak value of the cross correlation to determine the optimal position of the support constraint.

For the case of a difficult-to-reconstruct complex-valued object, initial attempts to use the small-aperture phase with the iterative Fourier-transform algorithm were unsuccessful, whether the phase was just used in the initial estimate or

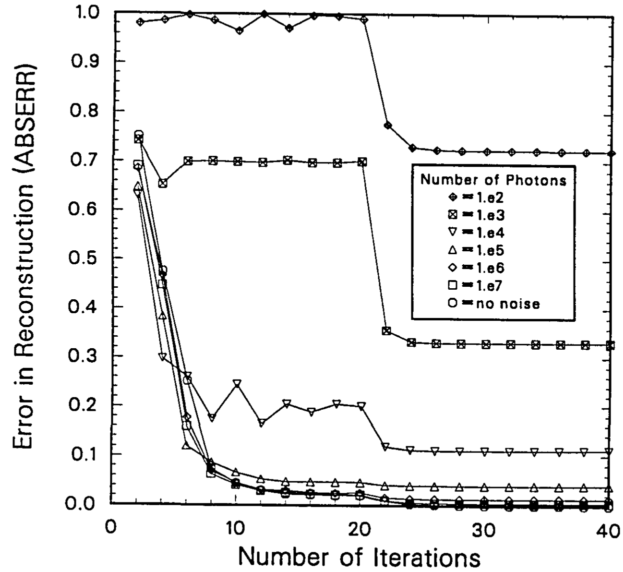

Fig. 8. Rms error (ABSERR) of the complex-valued reconstructed low-resolution image as a function of iteration number of a variety of light levels.

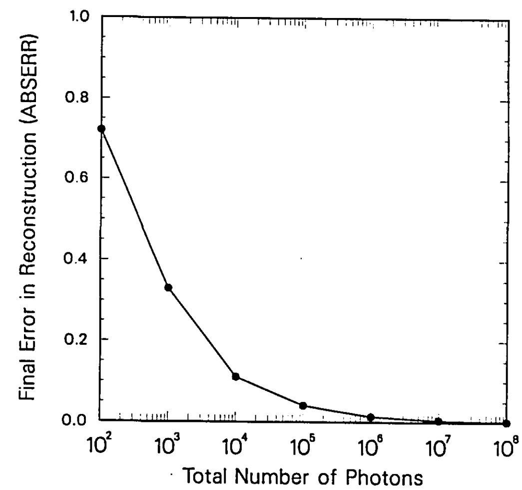

Fig. 9. Rms error of the complex-valued reconstructed low-resolution image as a function of light level.

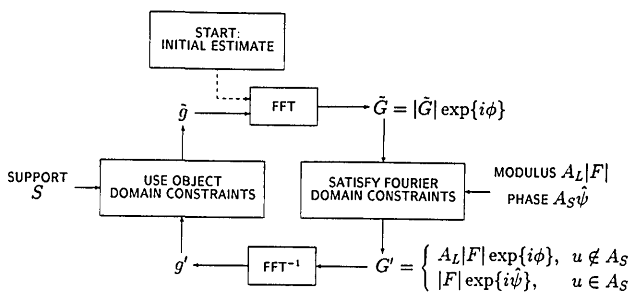

Fig. 10. Block diagram of the iterative Fourier-transform algorithm. The object-domain constraint is a support constraint derived from the measured data, and the Fourier-domain constraints are the square root of the measured intensity over the entire large aperture and the phase retrieved by the Gerchberg–Saxton algorithm over the small aperture.

reinforced during the iterations. A possible reason for this failure is the fact that the area of the small aperture is a small fraction of the area of the entire large aperture, and so the incorrect phase over the rest of the aperture overwhelms the influence that is due to the correct phase over the small aperture.

The following modifications to the algorithm were found to be necessary for a reliable reconstruction. First, in order to reduce impulse-response sidelobes it is advantageous to multiply the Fourier modulus by a weighting function. This is important since large sidelobes extending beyond the edges of the object support will violate the support constraint and hinder convergence. For ease of implementation, the Fourier modulus weighting function was chosen to be the autocorrelation of a circle. Initially the diameter of the circle was chosen to be such that the Fourier modulus weighting went to zero over an area just slightly larger than the area over which the small-aperture phase was known. Then a cycle of 30 hybrid input–output iterations (with feedback parameter $\beta = 0.7$) followed by 10 error-reduction iterations[1] was performed, reinforcing the phase over the small aperture at each iteration. Phase reinforcement is accomplished simply by replacing the phase of the Fourier transform of the input image by the (now) known phase over the area of the small aperture, while leaving the phase unchanged over the rest of the aperture. (In practice, reasonably good results can also be obtained if the phase over the small aperture is used for the first iteration only, without being reinforced during later iterations; but better results are obtained by continual reinforcement of the known phase.) This approach allowed the algorithm to converge to a solution for the phase over the nonzero area of the weighted Fourier modulus, since the phase was already known over most of that area to begin with. Then the Fourier modulus was reweighted with a weighting function of slightly larger area, and another cycle of iterations was performed. This process was continued until the weighting function encompassed the entire area of the measured Fourier modulus data. Thus the phase retrieval proceeded by a bootstrap approach, with successively larger areas of phase retrieved, and successively finer-resolution images reconstructed, during each cycle of iterations. When we compute the ABSERR by Eq. (3), we use for $g(x)$ the diffraction-limited image for the same weighting of the Fourier transform as is being used for the Fourier modulus weighting for that cycle of iterations. We recently learned that others have also found an expanding weighted modulus approach to be important for reconstructing images from noisy data.[21]

Ordinarily when reconstructions are performed with a poorly known support constraint (as is the case here), we find it best to start with a smaller support constraint for early iterations and expand the support constraint for later iterations. However, when the expanding weighted modulus algorithm is used, the images that are reconstructed during the early iterations are larger than the images reconstructed during the later iterations, since for the early iterations the point-spread function is much larger owing to the use of a narrow weighting function in the Fourier domain. By experimentation with support constraints that were expanded or shrunk as the iterations progressed, we found that a good strategy was to use a support constraint appropriate for the low-resolution image and keep it fixed during all the iterations. However, an alternative strategy may be necessary, depending on the ratio of the diameters of the small and large apertures or on how the support constraint is formed.

For fine-resolution image reconstruction from the Fourier modulus, for which the only image-domain constraint is a support constraint, the ODEM is given, instead of by Eq. (2), by

$$\mathrm{ODEM}^2 = \frac{\sum_{x \notin S} |g_k'(x)|^2}{\sum_{x} |g_k'(x)|^2}, \tag{5}$$

i.e., the energy outside the support constraint S.

4. IMAGE-RECONSTRUCTION EXAMPLE

Figure 11 shows an example of image reconstruction that uses the approach described above. Only the modulus of each complex-valued image is shown. Figure 11(A) shows the Fourier modulus data (noise free) over the entire aperture, a circle of diameter 64 pixels (embedded in a 128 × 128 array), with the aperture of the small telescope indicated by a dark circle. Figure 11(B) is the low-resolution image obtained through the small aperture of diameter 16 pixels,

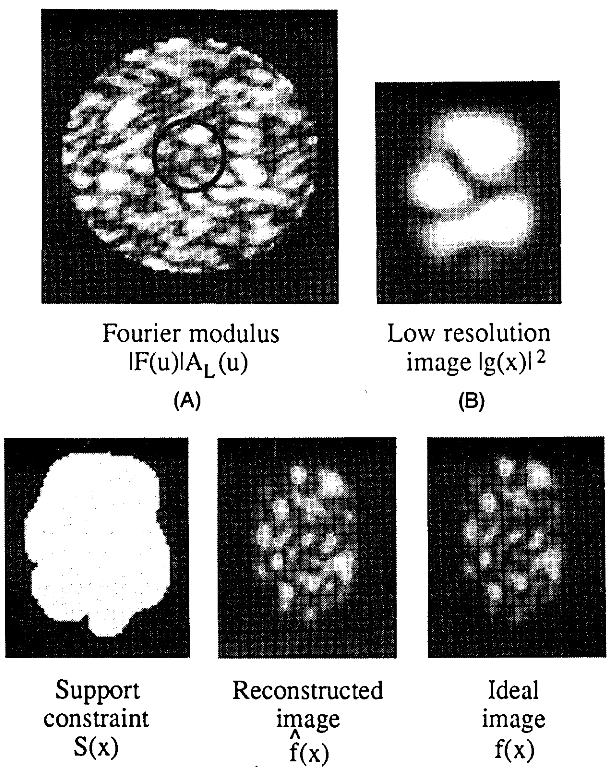

Fig. 11. Image-reconstruction example. (A) Fourier modulus data over a large circular aperture—the black circle shows the area of the small aperture, (B) low-resolution image from the small aperture, (C) object support constraint derived from (B), (D) image reconstructed by the Gerchberg–Saxton algorithm followed by the iterative Fourier-transform algorithm using (A)–(C), (E) ideal image for comparison.

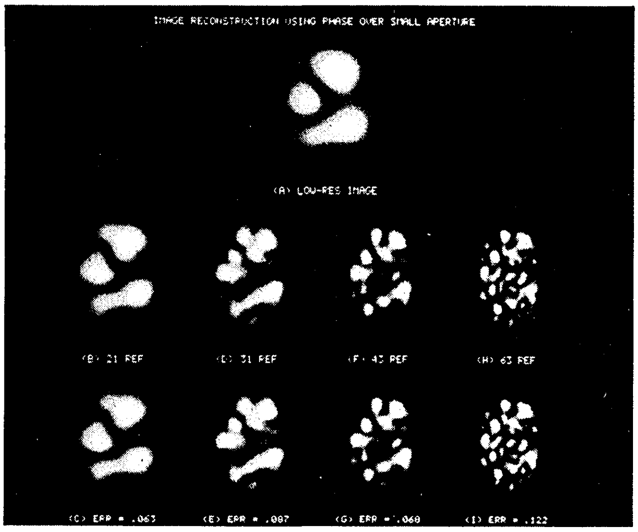

Fig. 12. Intermediate reconstruction results with different weightings on the Fourier modulus. Top row: low-resolution image from the small-aperture telescope; bottom row: intermediate reconstructed images; middle row: ideal images with the same Fourier weighting. Diameter of weighting function in pixels: (B), (C) 21; (D), (E) 31; (F), (G) 43; (H), (I) 63.

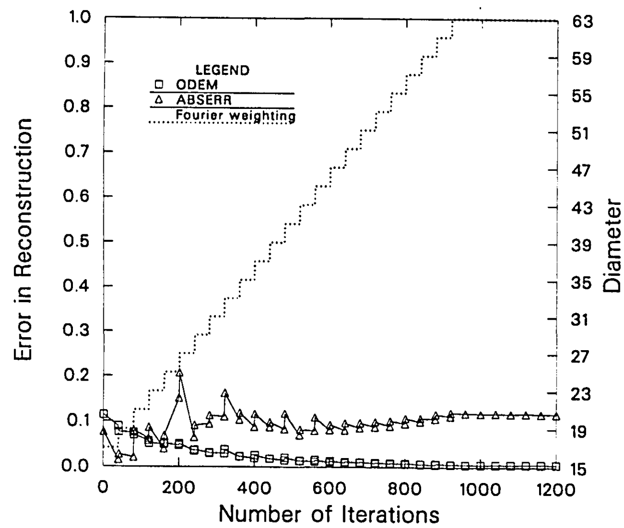

Fig. 13. Convergence of the iterative Fourier-transform algorithm: ODEM (□) and ABSERR (△) (solid curves, scale at left) and the diameter of the Fourier-modulus weighting function (dotted curve, scale at right) as a function of iteration number.

weighted by the autocorrelation of a diameter-8 circle. The support constraint, Fig. 11(C), was obtained by thresholding the low-resolution image as described above, and the small-aperture phase was estimated by the accelerated Gerchberg–Saxton algorithm. All that information—the Fourier modulus over the large aperture, the support constraint, and the Fourier phase over the small aperture—was combined to retrieve the phase over the large aperture by the iterative Fourier-transform algorithm, using the expanding weighted modulus approach. After 25 cycles of iterations during which the weighting was expanded, plus an additional 6 cycles at the end, for a total of more than 1000 iterations, the image shown in Fig. 11(D) was obtained. It is very close to the true fine-resolution diffraction-limited image shown in Fig. 11(D). Figure 12 shows intermediate results with different weightings on the Fourier modulus. The phase is retrieved well for each weighting of the Fourier modulus before the weighting function is expanded, and so at each step a diffraction-limited image (for the resolution given by the weighting function) is reconstructed. Figure 13 shows the ODEM and the ABSERR as a function of iteration number. Also indicated is the diameter of the Fourier-weighting function as the iterations progress. It was found that if substantially fewer iterations per cycle were used or if larger jumps in the size of the weighting function were used, then the convergence of the algorithm was much less reliable. Unlike in previously published results, in which the ODEM (or the ABSERR) starts out large and decreases with iteration number, here it starts low and stays low since at any given point we are trying to retrieve only an additional thin annulus of phase. A sawtooth behavior is seen since the error jumps up each time the weighting on the Fourier modulus is enlarged.

5. CONCLUSION

A complex-valued image of an object with convex support and without bright glints, whose support is not known *a priori*, is ordinarily difficult to reconstruct from its Fourier modulus. We have demonstrated that a low-resolution intensity image of the object, taken through a small-aperture telescope contiguous with intensity measurements over a large aperture, can be used to help to reconstruct a fine-resolution image. The low-resolution image is used both to determine the Fourier phase over the small aperture and to form a support constraint for the object. The retrieval of the phase over the small aperture, using an accelerated version of the Gerchberg–Saxton algorithm, was found to be not only fast but also robust in the presence of noise. The reconstruction of the fine-resolution image was also successful but was found to take a larger number of iterations and to require a bootstrapping approach using an expanding weighting function on the Fourier modulus. The determination of the algorithm's performance in the presence of noise will require further research, which is now being planned. However, based on earlier experience,[2,5] it can be expected to be less sensitive to noise than alternative approaches that employ zero sheets.[22,23]

APPENDIX A

We relate the variance of the error of an optical field (or the Fourier transform of a complex-valued image) to the variance of its phase error for a zero-mean Gaussian-distributed phase error.

Let

$$G(u) = F(u)\exp[i\phi_e(u)] \tag{A1}$$

be the aberrated optical field, where F is the ideal optical field and ϕ_e is the phase error. Suppose that ϕ_e has point statistics that are Gaussian zero mean with standard deviation σ_ϕ. First consider the case without normalizing G. Then the variance of the error (i.e., the mean-squared error) of $G(u)$ is

$$E^2 = A^{-1} \int |G(u) - F(u)|^2 d^2u$$
$$= A^{-1} \int |F(u)|^2 |1 - \exp[i\phi_e(u)]|^2 d^2u$$
$$= A^{-1} \int |F(u)|^2 4 \sin^2[\phi_e(u)/2] d^2u, \tag{A2}$$

where A is the area of integration. Assuming that the phase errors are independent of $|F(u)|$, and approximating the integral by an ensemble average, yields

$$E^2 \simeq 4\langle |F(u)|^2 \sin^2[\phi_e(u)/2]\rangle$$
$$\simeq 4\langle |F(u)|^2\rangle \langle \sin^2[\phi_e(u)/2]\rangle. \tag{A3}$$

With the identity[25]

$$\int_0^\infty \exp(-px^2)\sin^2(ax)dx = (1/4)\sqrt{\pi/p}\,[1 - \exp(-a^2/p)], \qquad p > 0, \tag{A4}$$

the average over the distribution of phases is given by

$$\langle \sin^2[\phi_e(u)/2]\rangle = \int_{-\infty}^{\infty} \sin^2(\phi_e/2) \frac{1}{\sqrt{2\pi}\sigma_\phi} \exp(-\phi_e^2/2\sigma_\phi^2) d\phi_e$$
$$= (1/2)[1 - \exp(-\sigma_\phi^2/2)]. \tag{A5}$$

Inserting Eq. (A5) into Eq. (A3) yields

$$e^2 \equiv \frac{E^2}{\langle |F(u)|^2\rangle} \simeq 2[1 - \exp(-\sigma_\phi^2/2)]. \tag{A6}$$

Note that $e^2 \to 2$ for $\sigma_\phi \to \infty$ and

$$e^2 \simeq \sigma_\phi^2 \qquad \text{for } \sigma_\phi^2 \ll 1. \tag{A7}$$

Next consider the case of a normalized G, as in Eq. (3):

$$E^2 = A^{-1} \int |\alpha G(u) - F(u)|^2 d^2u, \tag{A8}$$

where

$$\alpha = \frac{\int G^*(u')F(u')d^2u'}{\int |G(u'')|^2 d^2u''}. \tag{A9}$$

Then

$$\langle \alpha \rangle = \frac{\langle G^*F\rangle}{\langle |G|^2\rangle} = \frac{\langle |F|^2\rangle \langle \exp(-i\phi_e)\rangle}{\langle |F|^2\rangle} \tag{A10}$$
$$= \langle \exp(-i\phi_e)\rangle = \exp(-\sigma_\phi^2/2). \tag{A11}$$

Thus

$$E^2 \simeq A^{-1} \int |F(u)|^2 |\exp(-\sigma_\phi^2/2)\exp[i\phi_e(u)] - 1|^2 d^2u$$
$$= A^{-1} \int |F(u)|^2 \{\exp(-\sigma_\phi^2) + 1$$
$$-2 \exp(-\sigma_\phi^2/2)\cos[\phi_e(u)]\} d^2u$$
$$\simeq \langle |F(u)|^2\rangle \{\exp(-\sigma_\phi^2) + 1 - 2 \exp(-\sigma_\phi^2/2)\langle \cos[\phi_e(u)]\rangle\}$$
$$= \langle |F(u)|^2\rangle\, [\exp(-\sigma_\phi^2) + 1 - 2 \exp(-\sigma_\phi^2/2)\exp(-\sigma_\phi^2/2)]$$
$$= \langle |F(u)|^2\rangle [1 - \exp(-\sigma_\phi^2)] \tag{A12}$$

or

$$e^2 = \frac{E^2}{\langle |F(u)|^2\rangle} \simeq 1 - \exp(-\sigma_\phi^2). \tag{A13}$$

Note that for the normalized case, unlike the unnormalized case, $e^2 \to 1$ for $\sigma_\phi \to \infty$ and, like the unnormalized case, $e^2 \simeq \sigma_\phi^2$ for $\sigma_\phi^2 \ll 1$.

By Parseval's theorem it can be shown that the variance of the error in the image domain is equal to the variance of the error in the Fourier domain.

Just as image shifts can be taken out before computing errors to allow for the fact that image shifts are unimportant to image quality, linear components of the phase error $\phi_e(u)$ can be taken out before computing σ_ϕ or e^2.

ACKNOWLEDGMENTS

Portions of this paper were presented at the Optical Society of America Topical Meeting on Signal Recovery and Synthesis III, North Falmouth, Massachusetts, June 14–16, 1989.[24]

This research was supported by the U.S. Office of Naval Research and the Naval Research Laboratory.

REFERENCES

1. J. R. Fienup, "Reconstruction of a complex-valued object from the modulus of its Fourier transform using a support constraint," J. Opt. Soc. Am. A **4**, 118–123 (1987).
2. J. N. Cederquist, J. R. Fienup, C. C. Wackerman, S. R. Robinson, and D. Kryskowski, "Wave-front phase estimation from Fourier intensity measurements," J. Opt. Soc. Am. A **6**, 1020–1026 (1989).
3. T. R. Crimmins, J. R. Fienup, and B. J. Thelen, "Improved bounds on object support from autocorrelation support and application to phase retrieval," J. Opt. Soc. Am. A **7**, 3–11 (1990).
4. R. H. T. Bates and D. G. H. Tan, "Fourier phase retrieval when the image is complex," in *Inverse Optics II*, A. J. Devaney and R. H. T. Bates, eds., Proc. Soc. Photo-Opt. Instrum. Eng. **558**, 54–59 (1985).
5. R. G. Paxman, J. R. Fienup, and J. T. Clinthorne, "Effect of tapered illumination and Fourier intensity errors on phase retrieval," in *Digital Image Recovery and Synthesis*, P. S. Idell, ed., Proc. Soc. Photo-Opt. Instrum. Eng. **828**, 184–189 (1987).
6. R. G. Lane, "Recovery of complex images from Fourier magnitude," Opt. Commun. **63**, 6–10 (1987).
7. J. R. Fienup, "Reconstruction of an object from the modulus of its Fourier transform," Opt. Lett. **3**, 27–29 (1978).
8. J. R. Fienup, "Phase retrieval algorithms: a comparison," Appl. Opt. **21**, 2758–2769 (1982).
9. J. R. Fienup and C. C. Wackerman, "Phase retrieval stagnation problems and solutions," J. Opt. Soc. Am. A **3**, 1897–1907 (1986).
10. E. N. Leith and J. Upatnieks, "Reconstructed wavefronts and communication theory," J. Opt. Soc. Am. **52**, 1123–1130 (1962).
11. R. W. Gerchberg and W. O. Saxton, "A practical algorithm for the determination of phase from image and diffraction plane pictures," Optik **35**, 237–246 (1972).
12. W. O. Saxton, *Computer Techniques for Image Processing in Electron Microscopy* (Academic, New York, 1978).
13. J. R. Fienup, "Improved synthesis and computational methods for computer-generated holograms," Ph.D. dissertation, University Microfilms No. 75-25523 (Stanford University, Stanford, Calif., May 1975), Chap. 5.
14. J. R. Fienup, "Iterative method applied to image reconstruction and to computer-generated holograms," Opt. Eng. **19**, 297–305 (1980).
15. J. R. Fienup, "Reconstruction and synthesis applications of an iterative algorithm," in *Transformations in Optical Signal Processing*, W. T. Rhodes, J. R. Fienup, and B. E. A. Saleh, eds. Proc. Soc. Photo-Opt. Instrum. Eng. **373**, 147–160 (1981).

16. J. W. Goodman, *Introduction to Fourier Optics* (McGraw-Hill, New York, 1968).
17. R. Rolleston and N. George, "Image reconstruction from partial Fresnel zone information," Appl. Opt. **25,** 178–183 (1986).
18. J. R. Fienup, "Phase retrieval from Fourier intensity data," in *Digital Image Recovery and Synthesis*, P. S. Idell, ed., Proc. Soc. Photo-Opt. Instrum. Eng. **828,** 13–17 (1987).
19. J. W. Goodman, "Statistical properties of laser speckle patterns," in *Laser Speckle and Related Phenomena*, 2nd ed., J. C. Dainty, ed. (Springer-Verlag, New York, 1984), Chap. 2.
20. J. R. Fienup, T. R. Crimmins, and W. Holsztynski, "Reconstruction of the support of an object from the support of its autocorrelation," J. Opt. Soc. Am. **72,** 610–624 (1982).
21. B. C. McCallum and R. H. T. Bates, "Towards a strategy for automatic phase retrieval from noisy Fourier intensities," J. Mod. Opt. **36,** 619–648 (1989).
22. D. Izraelevitz and J. S. Lim, "A new direct algorithm for image reconstruction from Fourier transform magnitude," IEEE Trans. Acoust. Speech Signal Process. **ASSP-35,** 511–519 (1987).
23. R. G. Lane and R. H. T. Bates, "Direct phase retrieval," IEEE Trans. Acoust. Speech Signal Process. **ASSP-35,** 520–525 (1987).
24. J. R. Fienup and A. M. Kowalczyk, "Phase retrieval for a complex-valued object using a low-resolution image," in *Digest of Topcial Meeting on Signal Recovery and Synthesis III* (Optical Society of America, Washington, D.C., 1989), pp. 142–145.
25. I. S. Gradshteyn and I. M. Ryzhik, *Table of Integrals, Series, and Products, Corrected and Enlarged Edition* (Academic, New York, 1980), p. 480. Note that the earlier edition was in error.